The Journal of Chemical Physics

A density functional theory study of the adsorption behaviour of CO_2 on Cu_2O surfaces

Cite as: J. Chem. Phys. **145**, 044709 (2016); https://doi.org/10.1063/1.4958804
Submitted: 13 May 2016 . Accepted: 01 July 2016 . Published Online: 29 July 2016

Abhishek Kumar Mishra, Alberto Roldan, and Nora H. de Leeuw

View Online Export Citation CrossMark

ARTICLES YOU MAY BE INTERESTED IN

A consistent and accurate ab initio parametrization of density functional dispersion correction (DFT-D) for the 94 elements H-Pu
The Journal of Chemical Physics **132**, 154104 (2010); https://doi.org/10.1063/1.3382344

A climbing image nudged elastic band method for finding saddle points and minimum energy paths
The Journal of Chemical Physics **113**, 9901 (2000); https://doi.org/10.1063/1.1329672

CO_2 adsorption on TiO_2(101) anatase: A dispersion-corrected density functional theory study
The Journal of Chemical Physics **135**, 124701 (2011); https://doi.org/10.1063/1.3638181

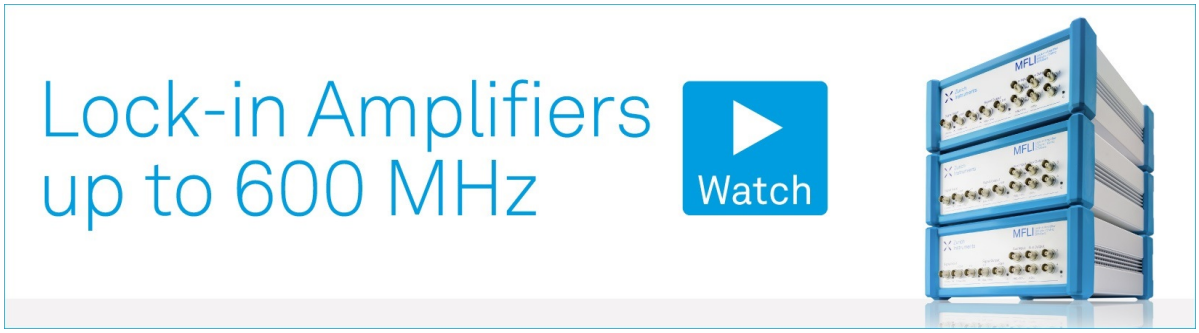

© 2016 Author(s).

THE JOURNAL OF CHEMICAL PHYSICS **145**, 044709 (2016)

A density functional theory study of the adsorption behaviour of CO_2 on Cu_2O surfaces

Abhishek Kumar Mishra,[1,2,a)] Alberto Roldan,[3] and Nora H. de Leeuw[2,3,a)]
[1]*Research & Development, University of Petroleum and Energy Studies (UPES), Bidholi, Dehradun 248007, India*
[2]*Department of Chemistry, University College London, 20 Gordon Street, London WC1H 0AJ, United Kingdom*
[3]*School of Chemistry, Cardiff University, Main Building, Park Place, Cardiff CF10 3AT, United Kingdom*

(Received 13 May 2016; accepted 1 July 2016; published online 29 July 2016)

Copper has many applications, particularly in electro-catalysis, where the oxidation state of the copper electrode plays a significant role in the selectivity towards products. Although copper-based materials have clear potential as catalysts in the reduction of CO_2 and conversion to products, fundamental understanding of CO_2 adsorption and activation on different copper oxide surfaces is still limited. We have used DFT+U methodology to study the surface reconstruction of the three most exposed (111), (110), and (001) surfaces of Cu_2O with different possible terminations. Considering several adsorbate geometries, we have investigated CO_2 adsorption on five different possible terminations and proposed eight different configurations in which CO_2 binds with the surface. Similar to earlier findings, CO_2 binds weakly with the most stable $Cu_2O(111)$:O surface showing no molecular activation, whereas a number of other surfaces, which can appear in the Cu_2O particles morphology, show stronger binding as well as activation of the CO_2 molecule. Different CO_2 coverages were studied and a detailed structural and electronic charge analysis is presented. The activation of the CO_2 molecule is characterized by structural transformations and charge transfer between the surface and the CO_2 molecule, which is further confirmed by considerable red shifts in the vibrational frequencies. © *2016 Author(s). All article content, except where otherwise noted, is licensed under a Creative Commons Attribution (CC BY) license (http://creativecommons.org/licenses/by/4.0/).* [http://dx.doi.org/10.1063/1.4958804]

I. INTRODUCTION

Copper is a unique metal owing to its ability to selectively produce hydrocarbons through the electro-reduction of CO_2,[1,2] where the oxidation state of the Cu electrode plays an important role in the product selectivity. The direct reduction of CO_2 to methanol (CH_3OH) is known to occur on oxidized Cu electrodes, which show an increase in the methanol formation by an order of magnitude compared to metallic copper.[3] The surface structure of oxidized copper resembles the Cu_2O (111)[4,5] surface and it reduces CO_2 to CH_3OH at rates remarkably higher than either air-oxidized or anodized Cu.[5] In addition, our recent density functional theory (DFT) based calculations of CO_2 hydrogenation on the most stable (111) surface of Cu_2O show that it is a suitable catalyst for CO_2 conversion to formate and formic acid under mild conditions.[6] Surface analysis of these oxides, before and after the reaction, shows mixed oxidation states (Cu_2O, Cu_4O_3, and CuO) depending on the method of preparation.[7] Recently, it has been demonstrated that CuO–Cu_2O nanorod arrays prepared on Cu substrates can drive the efficient solar photo-conversion of CO_2 to methanol.[8]

The catalytic process is affected considerably by the catalyst structure, with different shapes and surface arrangements having a large impact on the catalyst's activity and stability. Furthermore, surface structures and crystallographic facets of metal oxides have been found to control the gas sensing properties of metal oxide-based sensors.[9–11] By controlling the size and morphology, one can fine tune the strength of surface adsorption and reactivity to meet the stringent selectivity and activity requirements in a catalytic process. For example, our recent investigations of CO_2 activation on a number of Cu(II) oxide surfaces revealed that surface structures have significant effects on CO_2 activation and binding energies.[12]

The most exposed surfaces of Cu_2O are the (111), (110), and (001),[13] with the (111) surface the most stable and most studied among these surfaces.[14–19] However, shape-controlled synthesis of Cu_2O crystals has been investigated widely and a variety of morphologies has been synthesised successfully.[20–25] Recently, a study by Sun *et al.* on the crystal facet-dependent effect of polyhedral Cu_2O micro-crystals, that exposed different Miller index facets, showed that the catalytic performance can be enhanced by high-index facets,[26] Furthermore, copper(I) oxide nano clusters have been studied recently to understand the methanol formation through DFT based calculations.[27]

The adsorption of molecules on a catalyst surface is the first step in their activation and conversion in any catalytic process. CO_2 adsorption on the $Cu_2O(111)$ surface has been investigated by Wu *et al.*,[18,19] and Bendavid and Carter,[28] using

a)Electronic addresses: akmishra@ddn.upes.ac.in, abhishek.mishra@ucl.ac.uk, and deleeuwn@cardiff.ac.uk

 © Author(s) 2016.

DFT calculations. Wu *et al.*,[19] investigated CO_2 adsorption on the $Cu_2O(111)$ surface, using the standard generalized gradient approximation (GGA) and identified that CO_2 binds as a linear molecule in a tilted configuration to the surface, with its oxygen atom coordinated to a coordinatively unsaturated surface copper atom, releasing an adsorption energy of 26.8 kJ/mol. However, it is now well known that pure GGA can lead to considerable errors when calculating reactions where 3*d*-metal oxides are oxidized by means other than by oxygen. Reaction energies for these processes become more accurate when the so-called DFT+U method is applied.[29] Bendavid and Carter[28] recently investigated CO_2 adsorption on the $Cu_2O(111)$ using the DFT+U method and showed via comparison to adsorption energies derived by standard DFT that the U parameter is necessary. Their choice of U = 6 eV was based on their earlier work,[30] where they determined and compared different values of U to earlier DFT+U studies on Cu_2O and CuO.[31–33] The selection of their U value was based solely on its accuracy to predict the equilibrium lattice constant for Cu_2O. However, experimentally it is found that copper oxide surfaces consist of mixed Cu_2O and CuO surface species, whereas molecule interactions can also alter the oxidation state of the copper oxide surface, i.e., through −OH groups.[30] Therefore, we recently determined a single U parameter to describe adequately both Cu_2O and CuO in terms of experimental properties.[12] In the present work, we have employed DFT with this Hubbard U correction to explore CO_2 adsorption on different non-polar stoichiometric terminations of the (111), (110), and (001) surfaces of Cu_2O. We first describe the reconstruction of the different surfaces and their electronic properties, followed by a detailed discussion of the CO_2 adsorption behaviour.

II. COMPUTATIONAL DETAILS

All the calculations were performed using the Vienna *Ab initio* Simulation Package (VASP) with plane-wave basis set.[34–37] We have employed plane-wave DFT+U[38] with the PBE[39,40] exchange-correlation functional and the formalism of Dudarev *et al.*[38] The different Cu_2O surfaces were obtained by the METADISE code,[41] providing different non-polar surface terminations.[42] At the base of the surface simulation cell, two layers of atoms were fixed at their optimised bulk positions to simulate the bulk phase of the Cu_2O. Above these two layers, the surface is represented by three layers of atoms, whose positions are allowed to change freely during optimization. In each case, the vacuum region above the surface was 12 Å, i.e., large enough to avoid interactions between the periodic slabs. We sampled (1×1) and (2×2) supercells with $5 \times 5 \times 1$ and $3 \times 3 \times 1$ Monkhorst and Pack[43] k-point mesh, respectively. Such dense grids and a truncation kinetic energy of 450 eV for the plane waves ensured an accurate description of properties that are influenced by sharp features in the density of states. A total convergence better than 10^{-5} was reached and the interatomic forces were minimized to 0.01 eV/Å for structural relaxation calculations.

The surface energies of the relaxed slabs were obtained using a combination of calculations for the relaxed and unrelaxed surfaces. After surface relaxation, the top and bottom surfaces are not equivalent and therefore we also need to consider the unrelaxed surface energy (γ_u) in order to calculate the final surface energy of the relaxed surface. The unrelaxed surface energy is the surface energy before any surface optimisation and is calculated as

$$\gamma_u = \frac{E_{slab,u} - nE_{bulk}}{2A}, \tag{1}$$

where $E_{slab,u}$ is the energy of the unrelaxed slab, nE_{bulk} is the energy of an equal number of bulk atoms, and A is the surface area of one side of the slab. Using this value, it is then possible to calculate the relaxed surface energy (γ_r) from the total energy of the relaxed slab.

The relaxed surface energy, γ_r, is given by

$$\gamma_r = \frac{E_{slab,r} - nE_{bulk}}{A} - \gamma_u, \tag{2}$$

where $E_{slab,r}$ is the energy of the relaxed slab.

The equilibrium morphology of a Cu_2O particle (ignoring higher Miller indices) was constructed using Wulff's method,[44] which requires that the distance to a given surface from the center of the particle is proportional to the surface energy.

While modelling the CO_2 molecule, we have also used the implementation of the DFT-D2 approach described by Grimme[45] to account for long-range dispersion forces. The isolated molecule was modelled in the centre of a big cell with broken symmetry and lattice constants of 20 Å, sampling only the gamma-point of the Brillouin zone with the same accuracy parameters described for the surfaces.

The adsorption energy per molecule was calculated from the relation

$$E_{ads} = E_{surf+mol} - (E_{surf} + E_{mol}), \tag{3}$$

where $E_{surf+mol}$ is the total energy of the adsorbate-substrate system, E_{surf} is the energy of the naked surface slab, and E_{mol} is the energy of the isolated CO_2 molecule. Within this definition, a negative adsorption energy indicates an exothermic process.

III. RESULT AND DISCUSSION

In a recent work, we found that a value of U_{eff} = 7 eV results in the accurate reproduction of the structural parameters of Cu_2O and a proper description of the Cu(II) oxide.[12] At this U_{eff} value, we found the lattice parameter of Cu_2O to be 4.270 Å, which is very close to the experimental value of 4.2696 Å.[46] Other structural parameters were also found to be in close agreement with the experimental values.[46] We have therefore modelled the different Cu_2O surfaces using the same U_{eff} value and employing the same bulk structural parameters.[12]

A. Surface reconstructions

In this section (Sec. III A), we have described in detail the reconstruction of the different terminations of three low-index Cu_2O surfaces: (111), (110), and (001). We

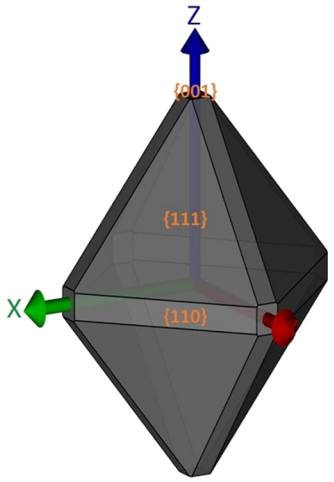

FIG. 1. The Wulff morphology of Cu_2O particle determined from calculated surface energies.

have calculated the surface energies of the different surface terminations from Equation (2) and determined the Wulff morphology[44] of the Cu_2O crystal, as shown in Fig. 1. The calculated surface energies (γ_r), the work functions, and the electronic band gaps of the different surfaces are listed in Table I.

1. *Cu_2O(111) surface*

a. (111):O. In agreement with Soon *et al.*,[47] we found that the most stable surface is the stoichiometric non-polar oxygen-terminated (111) surface, (111):O, with a surface energy of 1.08 J/m^2. The work function calculated with DFT+U is 4.98 eV, which is close to the experimental range of 4.62-4.84 eV.[48] This surface consists of four distinct types of atoms: unsaturated (singly coordinated) surface copper atoms Cu_{CUS}, outermost surface oxygens O_{SUF}, saturated copper atoms with linear O–Cu–O bond symmetry Cu_{CSA}, and sub-surface oxygens that are 4-fold coordinated O_{SUB} (Fig. 2). The unsaturated copper atoms (Cu_{CUS}) act as Lewis acid sites, where most of the surface reactions are believed to take place.[49]

After relaxation, the distance of the Cu_{CSA} atoms to O_{SUF} atoms decreases from 1.85 to 1.82 Å, but increases to the O_{SUB} atom to 1.86 Å. As a result, these Cu_{CSA} atoms become more exposed. The top Cu_{CUS} atoms also move outwards so that the vertical bond length between Cu_{CUS} and the topmost O atoms found in the second trilayer increases from 1.85 to 1.91 Å,

TABLE I. The calculated relaxed surface energies (γ_r), work functions (ϕ), and the bandgaps (E_g) of different Cu_2O surfaces.

Surface	γ_r (J/m^2)	ϕ (eV)	E_g (eV)
(111):O	1.08	4.98	0.78
(111):Cu	1.92	5.10	...
(110):Cu	1.24	5.41	0.30
(110):Cu–O	1.54	4.39	0.15
(100):Cu	1.62	4.54	...

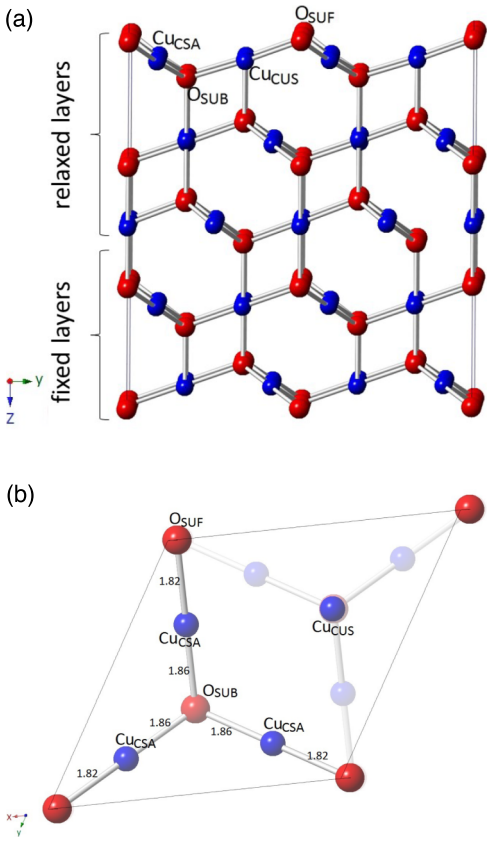

FIG. 2. The Cu_2O(111):O terminated relaxed surface side view (a) and top view (b). We have shown a (2×2) cell in side view with periodic images of atoms for clearer visualization of bonding in all surface figures. Blue and red balls indicate Cu and O atoms, respectively, in all figures. The bond length values are in Å.

while the vertical bond length from the sub-surface oxygen atoms to the copper atoms in the second layer also increases to 1.89 Å. We investigated the electronic density of states (DOS) (Fig. 3(a)) of this surface and found that the bandgap slightly decreases by 0.78 eV from the calculated value of 0.89 eV for the bulk Cu_2O material. The calculated values of the bandgap are expected to be under-estimated as DFT+U fails in the accurate prediction of bandgaps for Cu_2O.[12,32] The calculated projected DOS shows that both valence band maxima (VBM) and conduction band minima (CBM) mainly consist of O (2p) and Cu (3d) orbitals, respectively, while contributions from other orbitals are much less.

b. (111):Cu. We reconstructed another non-polar stoichiometric (111) surface with a Cu termination ((111):Cu), which, however, is found to be less stable by 0.84 J/m^2 than the (111):O surface. The work function is found to increase slightly to 5.10 eV. The presence of two Cu atoms at both top and bottom of the slab makes the (111):Cu surface non-polar, while maintaining the bulk Cu_2O ratio of Cu and O atoms (an unrelaxed (2 × 2) supercell is shown in Fig. S1 of the supplementary material). After relaxation, we noted significant changes in the positions of the top copper atoms, which moved down below the level of the O atoms. As a result, the O atoms in the relaxed surface are more exposed than the Cu atoms (Fig. 4). The Cu–O bond distance to these two Cu atoms increases slightly by 0.01 Å, while the vertical bond

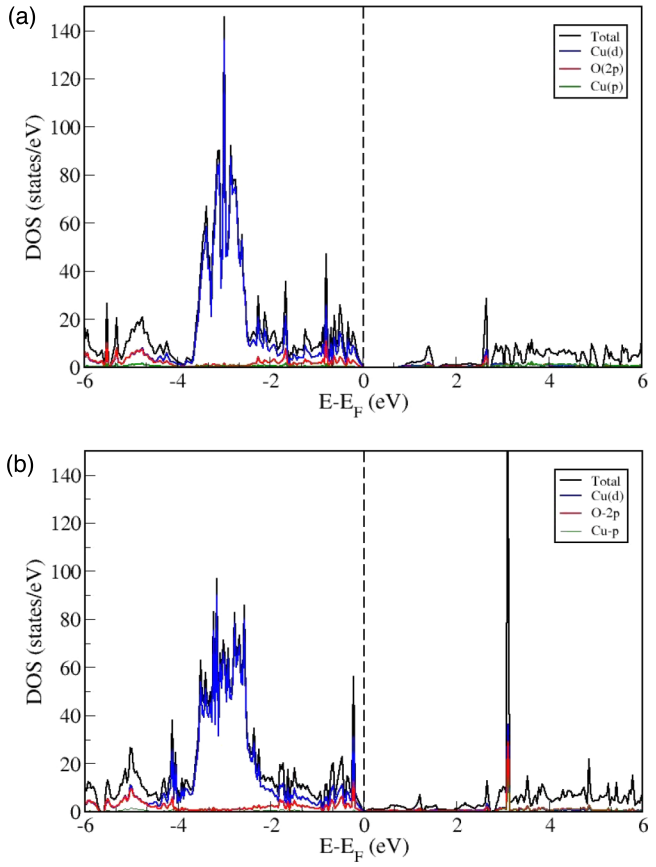

FIG. 3. Electronic DOS of Cu_2O (a) (111):O and (b) (111):Cu terminated surfaces with Fermi-level set to zero.

distance to the top O atoms from Cu atoms in the second layer decreases slightly by 0.01 Å. Other Cu–O bond distances in the second and third layers remain unchanged. We observed a finite number of states near the Fermi level in the electronic DOS of this surface and hence propose that this surface is conducting (Fig. 3(b)).

2. $Cu_2O(110)$ surface

a. (110):Cu. This surface consists of Cu atoms at the top of the first layer (Fig. S2 of the supplementary material) and hence we labelled this termination as (110):Cu. This is the second most stable surface with a surface energy of 1.24 J/m^2, while the work function is further increased to 5.41 eV. The top Cu atoms are connected to the 4-coordinated oxygen atoms (marked O_A), which are connected tetrahedrally to three more Cu atoms. The other type of O atoms (marked O_B) are 3-coordinated to copper atoms. After relaxation, these top copper atoms bend along the x-axis thereby increasing their distance to O_A atoms from 1.85 to 1.90 Å (Fig. 5). During the surface relaxation, the O_A atoms moved up, increasing the distance from the Cu atoms of the second layer from 1.85 to 1.91 Å. The O_B oxygens also move so that their distance to the lower Cu atoms changes to 1.84 from 1.85 Å. The bond length changes in the second layer are about 0.02 Å, while in the third layer they are less than 0.01 Å.

b. (110):Cu–O. In this termination, the surface consists of both Cu and O atoms at the top (labelled (110):Cu–O) and

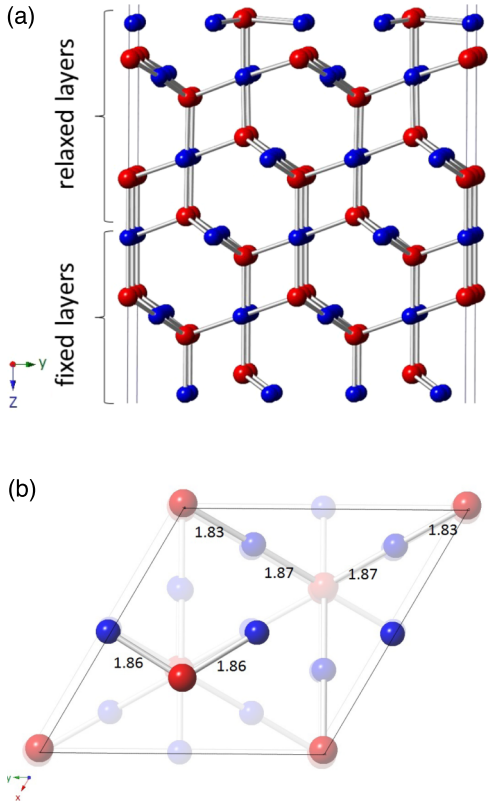

FIG. 4. The $Cu_2O(111)$:Cu terminated relaxed surface side (a) and top view (b). The bond length values are in Å.

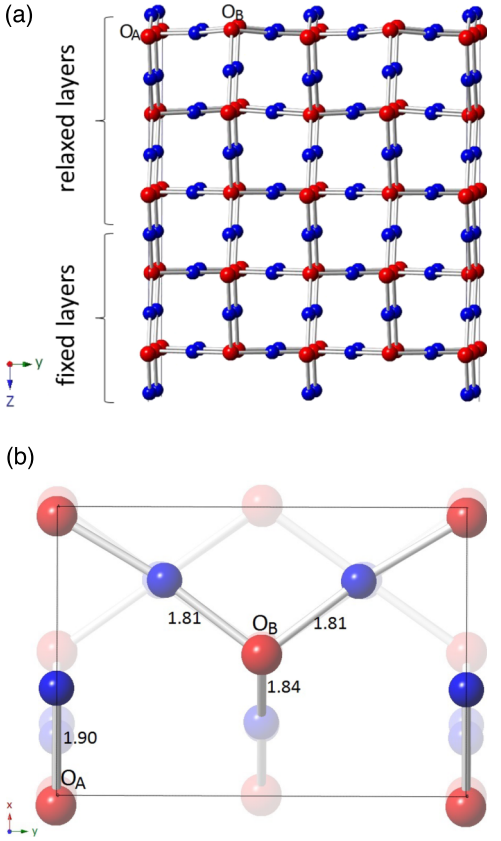

FIG. 5. The $Cu_2O(110)$:Cu terminated relaxed surface side (a) and top view (b). The bond length values are in Å.

the calculated surface energy is 1.54 J/m^2. The work function is found to be the lowest of the surfaces considered at 4.39 eV. During the reconstruction to remove the surface dipole, while keeping the ratio of Cu and O atoms the same as in the bulk, the oxygen atoms are rearranged at the top and bottom of the surface (Fig. S3 of the supplementary material). There are two distinct types of copper atoms below the top Cu–O layer, marked Cu_A and Cu_B. The Cu_A atoms are doubly coordinated to oxygens in the top and second layers, while the Cu_B atoms are only singly coordinated to an oxygen atom in the second layer. After relaxation, the top Cu and O atoms are closer and create weak Cu–O bonds of 2.10 and 2.18 Å in length (Fig. 6). The Cu_B type atoms are also rearranged and, after relaxation, these atoms connect with top O atoms (d_{CuB-O} = 1.87 Å).

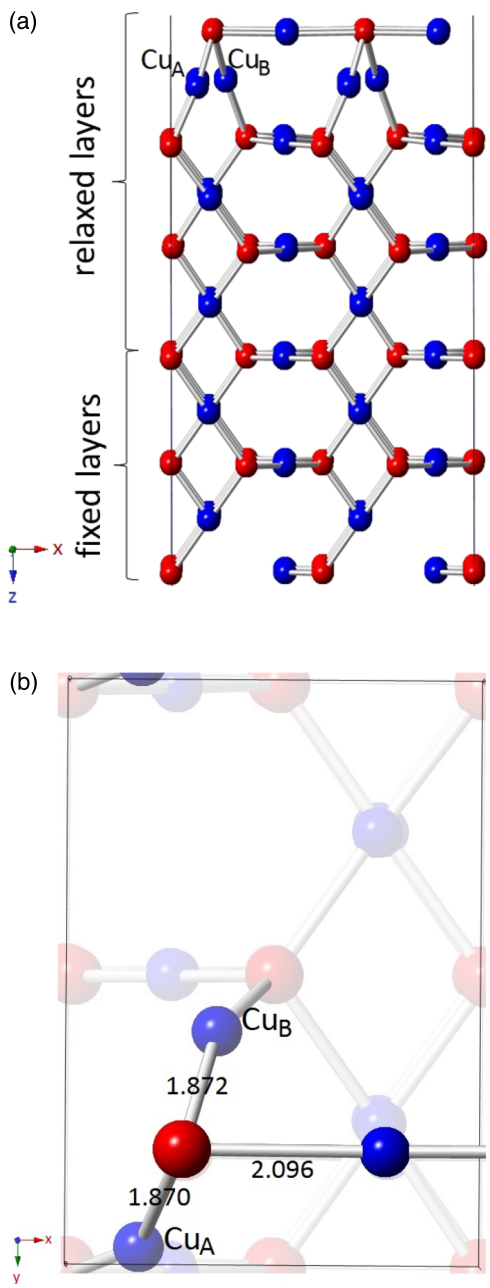

FIG. 6. The Cu_2O(110):Cu–O terminated relaxed surface side (a) and top view (b). The bond length values are in Å.

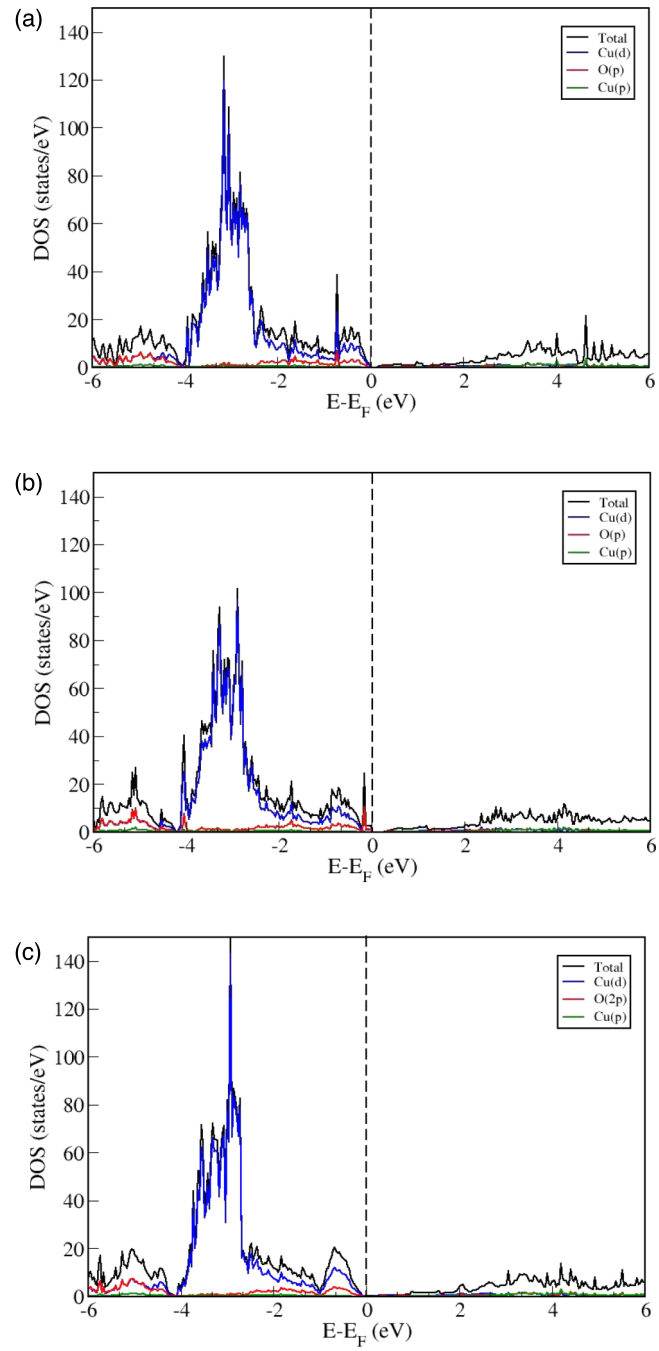

FIG. 7. Electronic DOS of Cu_2O (a) (110):Cu, (b) (110):Cu–O, and (c) (001):Cu terminated surfaces with Fermi-level set to zero.

The Cu–O bond distances in the second tri-layer increase up to 1.89 Å, while there are no structural changes in the third tri-layer.

We calculated the electronic DOS for both terminations and found that the bandgaps for the (110) surfaces are quite low, at 0.30 and 0.15 eV for the (110):Cu and (110):Cu–O terminations, respectively (Fig. 7).

3. Cu_2O(001) surface

a. (001):Cu. The (001):Cu is the only non-polar stoichiometric termination of the (001) surface. Its surface

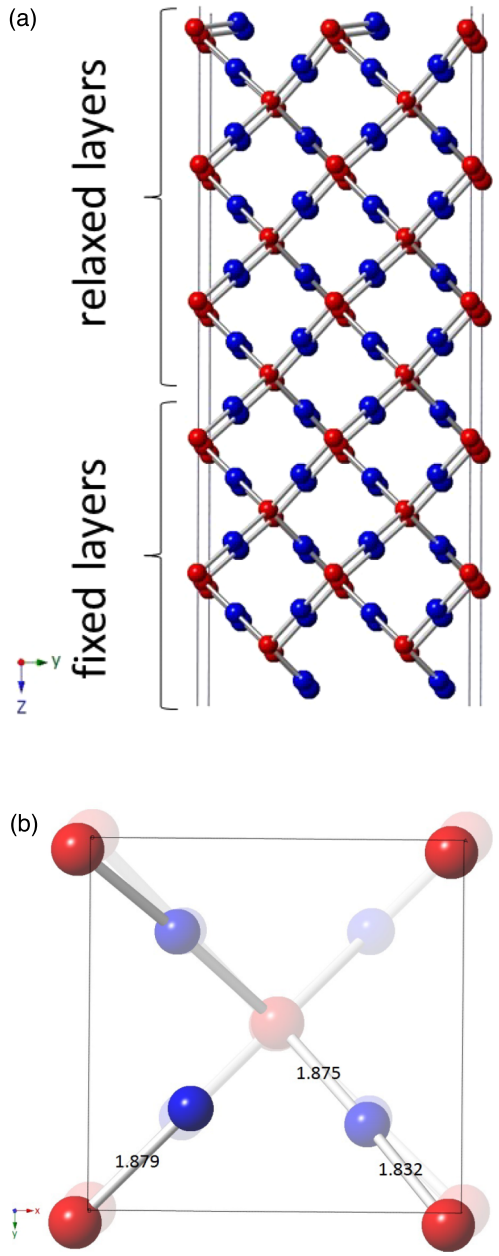

FIG. 8. The $Cu_2O(001)$:Cu terminated relaxed surface side (a) and top view (b). The bond length values are in Å.

energy is calculated at 1.62 J/m^2, which is 0.46 J/m^2 larger than the surface energy of the most stable $Cu_2O(111)$:O surface, while the work function is 4.54 eV. This surface consists of Cu atoms in the top layer connected to oxygen atoms below, which in turn are connected to two copper atoms in the layer below (Fig. S4 of the supplementary material). We noted that after relaxation, the top Cu atoms moved down and became less exposed and the Cu–O bond distance increased from 1.85 to 1.88 Å (Fig. 8). Cu atoms in the second layer move up to shorten the bond length to oxygen atoms in the top layer from 1.85 to 1.83 Å. We also noted that the Cu–O bond distance in all other relaxed surfaces increases from 1.85 Å and varies from 1.86 to 1.88 Å. With finite states near the Fermi level, this surface is also found to be conducting (Fig. 7).

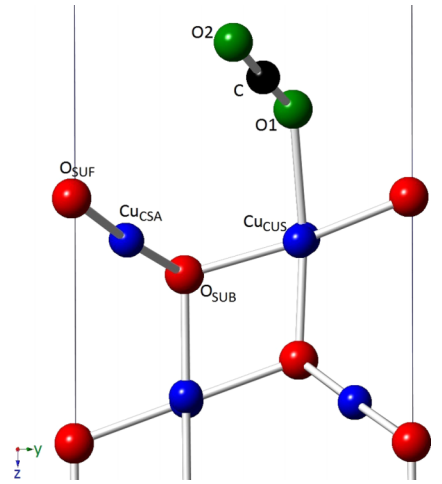

FIG. 9. The CO_2 molecule adsorbed on the $Cu_2O(111)$:O terminated surface. Black balls indicate C atom of CO_2 molecule, green balls indicate O atoms of the molecule, while blue and red balls denote the surface Cu and O atoms in all the figures.

B. CO_2 adsorption

1. $Cu_2O(111)$ surface

a. (111):O surface. A (1 × 1) slab (a = b = 6.04 Å) consists of 20 copper and 10 oxygen atoms. We first considered the (1 × 1) cell of the (111) surface for CO_2 adsorption and investigated a number of initial configurations with different orientations of the CO_2 molecule. We found that the CO_2 molecule moved away from the (111):O surface for all configurations, except where we placed it near the coordinatively unsaturated surface copper, Cu_{CUS}. In this configuration one of the oxygen atoms, O1, of the CO_2 molecule binds weakly with this Cu_{CUS} copper atom, as shown in Fig. 9. The CO_2 molecule remains almost linear with an angle of 176.9°. The distance between the oxygen atom O1 of the CO_2 molecule and Cu_{CUS} is found to be 2.05 Å, and the C–O bond between C and this O1 atom is slightly stretched at 1.19 Å, while the C–O2 bond length is found to be around 1.17 Å. Cu–O bond lengths in the slab also change slightly as a result of CO_2 adsorption, where the vertical bond distance between Cu_{CUS} (coordinated to the O1 atom of the CO_2 molecule) and the topmost O atom found in the second trilayer shortens from 1.91 to 1.88 Å. The adsorption energy in this configuration is −51.0 kJ/mol.

In order to assess the effect of CO_2 coverage, we repeated our calculation by placing one CO_2 molecule in a (2 × 2) supercell; we found that the adsorption energy increases to −56.1 kJ/mol, but with negligible changes in the CO_2 geometry. Adsorption geometries of the CO_2 molecule on

TABLE II. The adsorption energies and the characteristic parameter values of the CO_2 adsorbed geometry in the (1×1) and the (2×2) supercell of the $Cu_2O(111)$:O surface.

Supercell	E_{ads} (kJ/mol)	$\angle CO_2$ (deg)	d_{C-O1} (Å)	d_{C-O2} (Å)	$d_{O1-CuCUS}$ (Å)
(1×1)	−51.0	176.9	1.19	1.17	2.05
(2×2)	−56.1	178.3	1.18	1.18	2.05

TABLE III. Vibrational frequencies (cm^{-1}) and Bader charges (e^-) comparison of the atoms in the adsorbed CO_2 molecule and the $Cu_2O(111)$:O surface atoms bonded with the molecule to that of the atoms in the isolated CO_2 molecule and the bare surface in the (1×1) cell.

Atoms and vibrational modes	C	O1	O2	Cu_{CUS}	υ_{as}	υ_s	υ_b
Adsorbed CO_2 molecule	2.08	−1.07	−1.02	0.50	2332	1292	567
Isolated CO_2 molecule	2.08	−1.04	−1.04	...	2355	1316	632
Bare surface	...	...	...	0.44	...	...	...

both (1×1) and (2×2) supercell are given in Table II. Our calculated geometrical parameters of the adsorbed CO_2 molecule and the binding energies are in reasonable agreement with the recent work of Bendavid *et al.*, where they used similar DFT(D)+U (6 eV) methodology and found $\angle CO_2$ to be 177.1°and an adsorption energy of −36.4 kJ/mol.[28] This small change in adsorption energy value is expected as we have not included entropy and enthalpy energy corrections in our calculated adsorption energies.

A Bader charge analysis of the (1×1) cell (Table III) shows that the oxygen atom O1 of the CO_2 molecule (bonded to the coordinatively unsaturated surface copper Cu_{CUS}) gains $0.03e^-$, resulting from a small charge transfer from the surface copper atom Cu_{Cus}, which becomes more oxidized after CO_2 adsorption. This very small charge transfer between the surface and the CO_2 molecule, as well as small changes in vibrational frequencies (Table III) indicates weak activation of the CO_2 molecule.

b. (111):Cu surface. We calculated the CO_2 adsorption of numerous input configurations, placing the CO_2 molecule at different sites on the surface in different orientations, and we found that the CO_2 molecule binds in two configurations. In the first configuration (config. 1) after optimisation, the top Cu atoms Cu_A and Cu_B have moved upwards to interact with one of the CO_2 oxygen atoms O1, as shown in Fig. 10(a). The O1–Cu distances are 1.89 and 1.97 Å for Cu_A and Cu_B, respectively. The other oxygen atom, O2, of the CO_2 molecule remained unbound in this configuration. The CO_2 molecule bends with $\angle CO_2 = 125.5°$, as the carbon atom moved down to interact with a surface oxygen atom, O_{SUF}, in the second layer ($d_{C-OSUF} = 1.41$ Å). The C–O1 bond length becomes slightly elongated, $d_{C-O1} = 1.34$ Å, while the C–O2 bond is 1.22 Å long, i.e., longer than in the gas phase, which, together with the bending of the CO_2, is related to the activation of the molecule.[50] Upon CO_2 adsorption, the bond distance between the top Cu and O atoms changes from 1.86 Å to 1.83. We

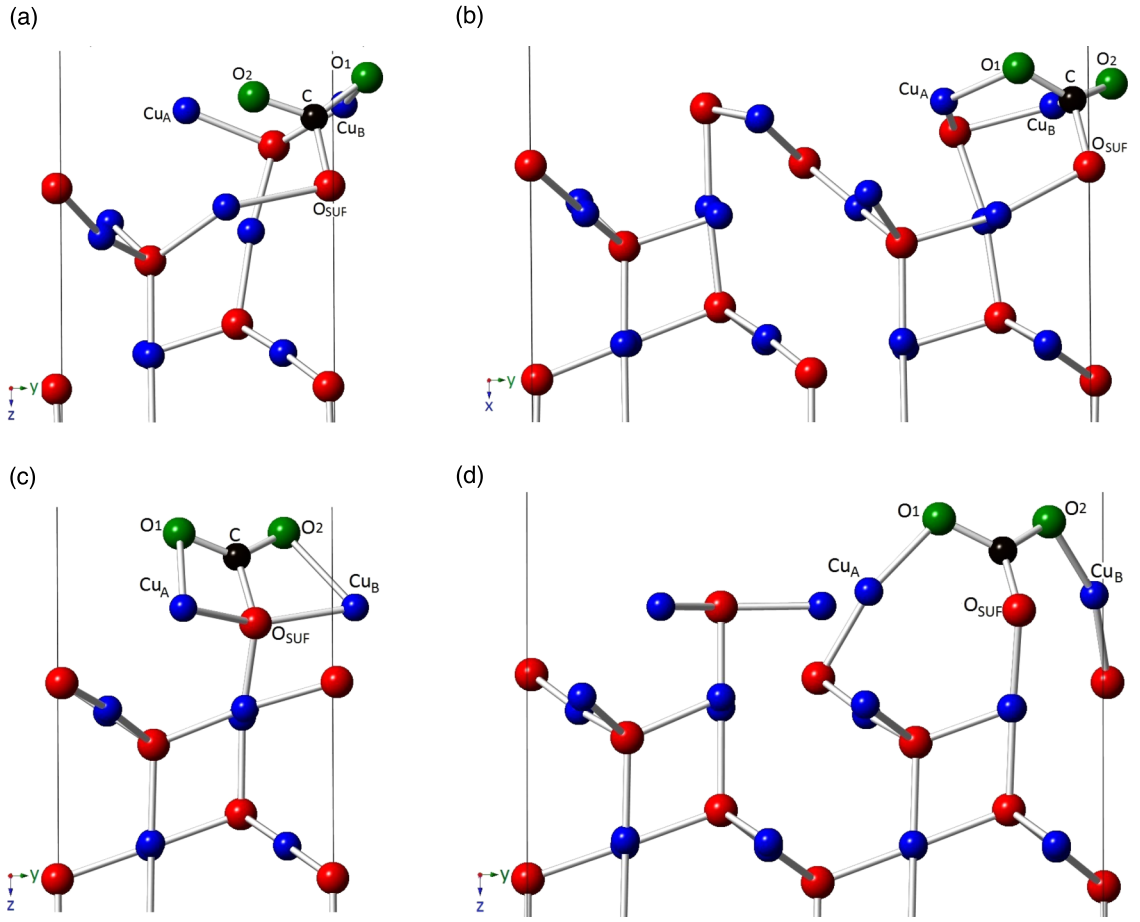

FIG. 10. The CO_2 molecule adsorbed on the $Cu_2O(111)$:Cu terminated surface in the (a) (1×1) cell, (b) (1×2) supercell in config. 1 and in the (c) (1×1) cell, (d) (1×2) supercell in config. 2.

TABLE IV. The adsorption energies and the characteristic parameter values of the CO_2 adsorbed geometry in the (1×1) and the (1×2) supercell of the $Cu_2O(111)$:Cu surface in config. 1 and config. 2.

Supercell	E_{ads} (kJ/mol)	$\angle CO_2$ (deg)	d_{C-O1} (Å)	d_{C-O2} (Å)	d_{O1-CuA} (Å)	d_{O1-CuB} (Å)	d_{C-OSUF} (Å)
Config. 1							
(1×1)	−117.1	125.5	1.34	1.22	1.89	1.97	1.41
(1×2)	−161.5	129.0	1.27	1.27	1.91	1.90	1.42
Config. 2							
(1×1)	−97.1	133.2	1.26	1.26	2.14	2.14	1.44
(1×2)	−232.6	119.2	1.30	1.30	1.85	1.85	1.32

noted that the surface oxygen atoms, which were connected in a vertical linear manner to Cu and O atoms in the second and third layer, respectively, bend towards the CO_2 molecule with loss of linearity. The adsorption energy calculated in this configuration is −117.1 kJ/mol.

We noted that due to the orientation of the CO_2 molecule, the lateral distance in the x-direction between the CO_2 molecule and its periodic image is 6.04 Å, while in the y-direction, it is only 3.80 Å. Hence, to minimize the effect of the periodic images on the CO_2 adsorption, we carried out calculations on a (1 × 2) supercell. At this lower coverage, CO_2 adsorbs in a slightly different manner, as the top surface Cu atoms (Cu_A and Cu_B) interact with both CO_2 oxygen atoms at distances of 2.03 Å and 2.01 Å, respectively (Fig. 10(b)). As a result, the Cu_A and Cu_B bond lengths with oxygen atoms in the surface change to 1.91 and 1.90 Å, respectively. Because of the lower coverage of CO_2 molecules on the surface, other surface Cu atoms (further away from the CO_2 molecule) bend inwards to bind to O atoms in the second layer, as shown in Fig. 10(b). As expected, the adsorption energy increases to about −161.5 kJ/mol. Similar to the (1 × 1) cell configuration, the C atom of the CO_2 molecule bends towards a surface oxygen atom O_{SUF} in the second layer (d_{C-OSUF} = 1.42 Å). The angle of the adsorbed CO_2 molecule is 129.0° and both C–O bond lengths are 1.27 Å. We have given parameters of the CO_2 adsorption geometries in the (1 × 1) and (1 × 2) simulation cells in Table IV.

Bader charge analysis of the (1 × 2) supercell shows charge transfer between the CO_2 molecule and the surface, as both molecular oxygens O1 and O2 gain $0.08e^-$ and $0.07e^-$ charge densities, respectively. This charge transfer originates mainly from the interacting surface copper atoms Cu_A and Cu_B, which become more positively charged after adsorption. The O_{SUF} atom bound to the molecule also gains $0.11e^-$ charge density (Table V). We also note some charge redistribution on the Cu_2O surface as a result of CO_2 adsorption. Bader analysis indicates the CO_2 molecule as a chemisorbed anion on the surface, in agreement with the molecular orbital occupation and bending of the molecule. This activation of the CO_2 molecule is also reflected in terms of changes in the vibrational frequencies of the molecule, as asymmetric (υ_{as}) and symmetric (υ_s) stretching modes change to 1560 and 1200 cm^{-1} from their values of 2355 and 1316 cm^{-1}, respectively, in the isolated gas phase molecule (Table V).

In a different configuration (config. 2), CO_2 binds to the (111):Cu terminated surface through its C atom to a surface oxygen atom (d_{C-OSUF} = 1.44 Å), while both oxygen atoms of the molecule bind to Cu_A and Cu_B (d_{O-Cu} = 2.14 Å), as shown in Fig. 10(c). The CO_2 molecule again bends to $\angle CO_2$ = 133.2°, while the Cu–O–Cu angle in the surface is about 145.4°. We found the surface Cu–O bonds to be slightly more stretched with bond distances of 1.98 Å. The adsorption energy at this coverage is −97.1 kJ/mol, which is slightly less than the same coverage in config. 1. Similar to config. 1, we also investigated a lower coverage of CO_2 at the surface in a (1 × 2) supercell (Fig. 10(d)). At this coverage, after CO_2 adsorption, surface rearrangement takes place where copper atoms Cu_A and Cu_B break their bonds with the O_{SUF} atom to form new bonds to surface oxygen atoms nearby, as well as bind to both CO_2 oxygen atoms (d_{O-Cu} = 1.85 Å). The carbon atom binds more strongly to surface atom O_{SUF} (d_{C-OSUF} = 1.32 Å) as the CO_2 angle changes to $\angle CO_2$ = 119.0°, and we noted that $\angle O_1$–C–O_{SUF} and $\angle O_2$–C–O_{SUF} are ∼120.0°. The adsorption energy increases to −232.6 kJ/mol (Table IV). Despite this large adsorption energy, Bader charge comparison (Table V) of the free CO_2 molecule with that in the adsorbed geometry shows that there is very little charge transfer, although large charge redistribution takes place among the surface atoms bonded to the molecule. O_{SUF} atom gains $0.23e^-$ charge

TABLE V. Vibrational frequencies (cm^{-1}) and Bader charges (e^-) comparison of the atoms in the adsorbed CO_2 molecule and the $Cu_2O(111)$:Cu surface atoms bonded with the molecule in the (1×2) supercell to that of the atoms in the isolated CO_2 molecule and the bare surface in config. 1 and config. 2.

Atoms and vibrational modes	C	O1	O2	Cu_A	Cu_B	O_{SUF}	υ_{as}	υ_s	υ_b
After CO_2 adsorption (config. 1)	2.02	−1.12	−1.11	0.54	0.55	−1.03	1560	1200	748
After CO_2 adsorption (config. 2)	2.09	−1.06	−1.07	0.56	0.58	−1.15	1395	1257	858
Isolated CO_2 molecule	2.08	−1.04	−1.04	...	...	...	2355	1316	632
Bare surface	...	...	...	0.41	0.40	−0.92	...	...	...

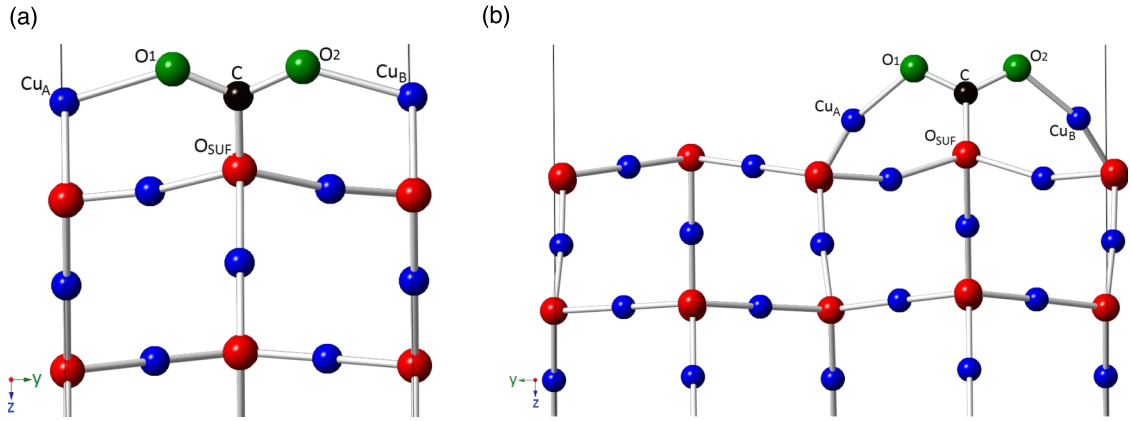

FIG. 11. The CO_2 molecule adsorbed on the Cu_2O(110):Cu terminated surface in the (a) (1×1) cell and in the (b) (1×2) supercell.

density, while Cu_A and Cu_B both lose $0.16e^-$ and $0.17e^-$ in charge densities, respectively. This charge redistribution together with the change in the surface results in a CO_3^- like-species on the (111):Cu surface (Fig. 10(d)). Unstable surfaces are often highly reactive, which is exemplified by this behaviour of the (111):Cu surface. This strong activation of the CO_2 molecule is further confirmed by considerable changes in the vibrational modes of the adsorbed CO_2 molecule, where asymmetric stretch (υ_{as}), symmetric stretch (υ_s), and bending (υ_b) frequencies change to 1395, 1257, and 858 cm^{-1}, respectively, from their original values of 2355, 1316, and 632 cm^{-1} in the isolated gas phase molecule.

2. *Cu_2O(110) surface*

a. (110):Cu. For this surface, we first considered a (1 × 1) unit cell and tried different initial configurations with several orientations of the CO_2 molecule, but we found only one configuration in which CO_2 binds to the surface. Here, CO_2 binds strongly (E_{ads} = −100 kJ/mol) in a configuration where the molecule bends to bind with an oxygen atom in the second layer (d_{C-OSUF} = 1.45 Å), while its oxygen atoms O1 and O2 bind to surface atoms, Cu_A and Cu_B, at 1.97 Å (Fig. 11(a)). We noted that the CO_2 molecule is activated with an angle of $\angle CO_2$ = 128.0°. From Fig. 11(a), we observe that the distance between the CO_2 molecule and its image in the x-direction is 4.3 Å, while in the y-direction it is only 3.78 Å. We therefore repeated the calculations of all the different configurations in (2 × 1) and (1 × 2) supercells.

Keeping the same input orientations, we first assessed the effect of a lower CO_2 coverage by placing one molecule in a (2 × 1) supercell and found that E_{ads} increased to −105.0 kJ/mol, while in the (1 × 2) supercell, E_{ads} increased to −116.7 kJ/mol. This increase in E_{ads} was expected because of the small distance between the CO_2 molecule and its periodic image in the y-direction in the (1 × 1) cell. Because of the significant difference in E_{ads} in the (1 × 2) supercell compared to the (2 × 1) supercell, we have limited our discussion only to the more favourable (1 × 2) supercell system. In the (1 × 2) supercell, the carbon atom of the molecule binds strongly to the surface oxygen atom (d_{C-OSUF} = 1.42 Å), while Cu_A–O1 and Cu_B–O2 bond lengths reduce to 1.89 Å (Fig. 11(b)). We have given geometrical parameters of the adsorbed geometry of the (1 × 1) and (1 × 2) supercells in Table VI. Bader analysis of the (1 × 2) supercell (Table VII) shows charge transfer between the oxygen atoms of CO_2 and surface copper atoms. Oxygen atoms O1 and O2 gain 0.05 and $0.06e^-$, respectively, while both surface copper atoms Cu_A and Cu_B lose $0.12e^-$. There is a very small charge transfer to the carbon atom of the CO_2 molecule of $\sim 0.01e^-$. This amount of charge transfer is consistent with the charge transfer in the (111):Cu surface, where the molecule's oxygen gains $\sim 0.08e^-$ and surface copper atoms lose charge of $\sim 0.15e^-$. Here also, frequencies for asymmetric stretch (υ_{as}), symmetric stretch (υ_s), and bending (υ_b) vibrations change to 1639, 1247, and 808 cm^{-1}, indicating activation of the CO_2 molecule on the (110):Cu surface. In all other configurations considered, the CO_2 molecule does not bind to the copper oxide surface.

b. (110):Cu–O. Here again, we carried out calculations on a (2 × 1) supercell, exploring different configurations for CO_2 to bind with the surface. In the first configuration (config. 1), after placing the CO_2 molecule parallel to the Cu–O–Cu linear bond in the top layer, we found that this bond breaks when Cu atoms move up to bind to oxygen atoms of the CO_2 molecule, while the carbon atom bends down to bind to the oxygen atom of the top surface layer (d_{C-OSUF} = 1.36 Å), as shown in Fig. 12(a). One of the CO_2 oxygen atoms (O1) binds to one of the nearest Cu atoms (Cu_A) in the top layer with a bond distance d_{O1-CuA} = 1.84 Å, while the second oxygen (O2) binds to another surface copper atom with a bond distance d_{O2-CuB} = 1.86 Å, causing the Cu–O distances of Cu_A and Cu_B to their neighbouring surface oxygen atoms to change from 2.10 and 2.18 Å to 1.83 and 1.84 Å, respectively. The CO_2 molecule bends to an angle of $\angle CO_2$ = 123.6° and adsorbs strongly with an adsorption

TABLE VI. The adsorption energies and the characteristic parameter values of the CO_2 adsorbed geometry in the (1×1) and the (1×2) supercell of the Cu_2O(110):Cu surface.

Supercell	E_{ads} (kJ/mol)	$\angle CO_2$ (deg)	d_{C-O1} (Å)	d_{C-O2} (Å)	d_{O1-CuA} (Å)	d_{O1-CuB} (Å)	d_{C-OSUF} (Å)
(1×1)	−100.4	128.0	1.26	1.26	1.97	1.97	1.45
(1×2)	−116.7	126.2	1.26	1.26	1.89	1.89	1.42

TABLE VII. Vibrational frequencies (cm^{-1}) and Bader charges (e^-) comparison of the atoms in the adsorbed CO_2 molecule and the $Cu_2O(110)$:Cu surface atoms bonded with the molecule to that of in the isolated CO_2 molecule and the bare surface in the (1×2) supercell.

Atoms and vibrational modes	C	O1	O2	Cu_A	Cu_B	O_{SUF}	υ_{as}	υ_s	υ_b
After CO_2 adsorption	2.07	−1.09	−1.10	0.56	0.56	−1.04	1639	1247	808
Isolated CO_2 molecule	2.08	−1.04	−1.04	...	...	...	2355	1316	632
Bare surface	...	...	...	0.44	0.44	−0.95	...	...	...

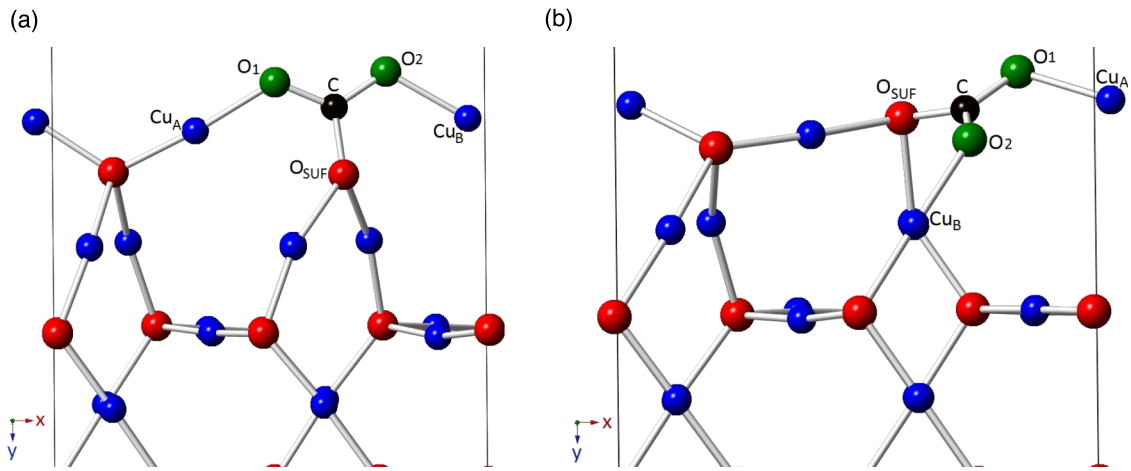

FIG. 12. The CO_2 molecule adsorbed on the $Cu_2O(110)$:Cu–O terminated surface in the (2×1) cell in (a) config. 1 and (b) config. 2.

energy E_{ads} = −138.1 kJ/mol. In this configuration, the C–O bond length is 1.27 Å, which is slightly longer than the normal bond length in a CO_2 molecule. The adsorption energy and geometrical parameters of the system are given in Table VIII. Bader charge analysis (Table IX) reveals that the O1 and O2 oxygen atoms of the CO_2 molecule gain 0.13 and 0.10e^- in charge density, respectively. Meanwhile, the surface copper atoms, Cu_A and Cu_B, which are bound to the O1 and O2 lose a charge density of 0.49 and 0.39e^-, respectively, while the surface oxygen atom (O_{SUF}) bound to the carbon atom of the CO_2 molecule gains 0.14e^-. Hence, upon CO_2 adsorption, a large charge redistribution occurs at the surface. This strong adsorption and activation of the CO_2 molecule are reflected in changes in the vibrational frequencies, as listed in Table IX.

In the second configuration (config. 2) (Fig. 12(b)), the carbon atom binds to the O_{SUF} atom (d_{C-OSUF} = 1.35 Å) and O1 binds to Cu_A (d_{O1-CuA} = 1.85 Å) in the top layer. The CO_2 molecule bends so that O2 binds with Cu_B of the second layer (d_{O2-CuB} = 1.86 Å), as shown in Fig. 12(b). In this configuration, we found that CO_2 binds more strongly with an adsorption energy of about −170.0 kJ/mol. CO_2 bends to an angle of $\angle CO_2$ = 122.7° which indicates stronger activation (Table VIII). Oxygen–carbon bond lengths, i.e., d_{C-O1} and d_{C-O2}, are found to be 1.27 Å and 1.30 Å, respectively. After CO_2 adsorption, the Cu–O bonds in the top of the surface change from 2.10 Å and 2.18 Å to 1.86 Å and 1.82 Å for Cu_A and Cu_B, respectively. Bader charge analysis (Table IX) shows that the oxygen atoms O1 and O2 of the CO_2 molecule gain −0.13 and −0.08e^-, respectively, while the change in the carbon atom charge is negligible. The surface copper atom Cu_A bonded to one of the oxygen atoms of the CO_2 molecule becomes more positively charged with a loss of 0.26e^-, while the surface oxygen atom O_{SUF} gains 0.23e^-. Charge transfer to Cu_B is negligible. This charge transfer, the adsorption energy, geometry changes together with large changes in vibrational frequencies (Table IX) indicates activation of the CO_2 molecule.

TABLE VIII. The adsorption energies and the characteristic parameter values of the CO_2 adsorbed geometry in the (2×1) supercell of the $Cu_2O(110)$:Cu–O surface in config. 1 and config. 2.

Supercell	E_{ads} (kJ/mol)	$\angle CO_2$ (deg)	d_{C-O1} (Å)	d_{C-O2} (Å)	d_{O1-CuA} (Å)	d_{O2-CuB} (Å)	d_{C-OSUF} (Å)
Config. 1							
(2×1)	−138.1	123.6	1.27	1.27	1.84	1.86	1.36
Config. 2							
(2×1)	−169.9	122.7	1.27	1.30	1.85	1.86	1.35

3. *$Cu_2O(001)$ surface*

a. (001):Cu. The (1 × 1) cell (a = 4.27 Å, b = 4.27 Å) is too small to study adsorption of the isolated molecule, as we discovered earlier that the interaction between neighbouring CO_2 molecules affects the geometry and adsorption energies. Hence, we carried out calculations on the (2 × 2) supercell to minimize the effect of interactions between periodic images. Similar to the other surfaces, we studied different sites at the surface for possible CO_2 adsorption. In the first adsorption configuration (config. 1), oxygens O1 and O2 of the molecule bind to the nearest topmost copper atoms

TABLE IX. Vibrational frequencies (cm^{-1}) and Bader charges (e^-) comparison of the atoms in the adsorbed CO_2 molecule and the $Cu_2O(110)$:Cu–O surface atoms bonded with the molecule to that of in the isolated CO_2 molecule and the bare surface in config. 1 and config. 2 of (2×1) supercell.

Atoms and vibrational modes	C	O1	O2	Cu_A	Cu_B	O_{SUF}	υ_{as}	υ_s	υ_b
After CO_2 adsorption (config. 1)	2.07	−1.14	−1.17	0.91	0.81	−1.03	1580	1291	869
After CO_2 adsorption (config. 2)	2.07	−1.17	−1.12	0.53	0.69	−1.12	1508	1250	851
Isolated CO_2 molecule	2.08	−1.04	−1.04	...	...	...	2355	1316	632
Bare surface	...	...	...	0.42	0.42	−0.89	...	...	...

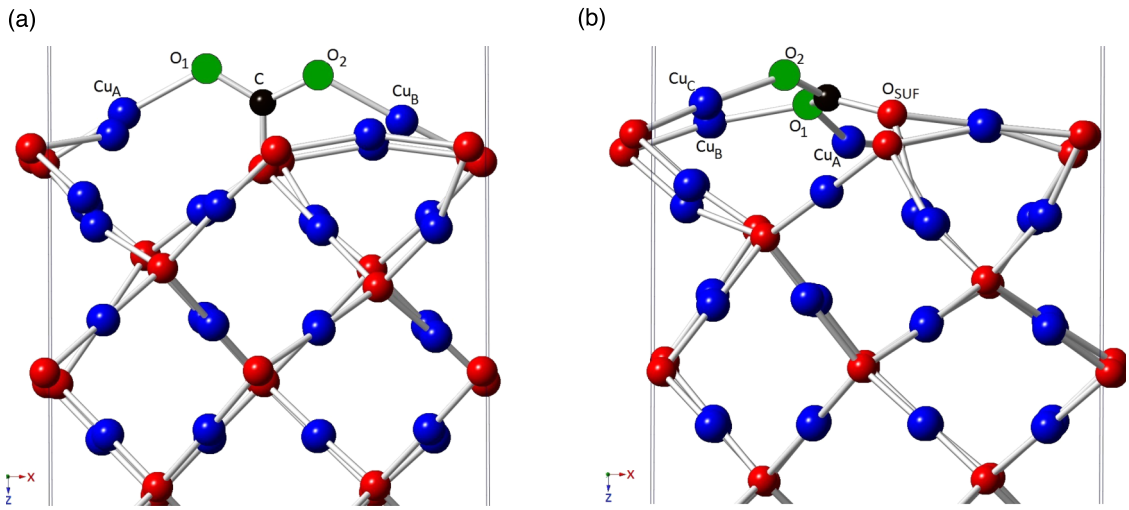

FIG. 13. The CO_2 molecule adsorbed on the $Cu_2O(001)$:Cu terminated surface in the (2×2) cell in (a) config. 1 and (b) config. 2.

Cu_A and Cu_B with bond distances of 1.85 and 1.87 Å, respectively (Fig. 13(a)). The CO_2 molecule bends to an angle of 121.5° as the carbon atom moves down to bind with the nearest available oxygen atom (O_{SUF}) of the top layer with a bond length d_{C-OSUF} of 1.35 Å. Upon CO_2 adsorption, the bond between Cu_B and O_{SUF} is broken, as shown in Fig. 8(a). The adsorption energy, E_{ads}, calculated for this configuration is −138 kJ/mol. Carbon–oxygen bond lengths in the CO_2 molecule are found to be 1.29 and 1.28 Å for O1 and O2, respectively. Copper–oxygen bond lengths in the surface for Cu_A and Cu_B change from 1.88 to 1.84 Å and 1.86 Å, respectively (Table X). Bader charge analysis (Table XI) shows significant charge transfer between the CO_2 molecule and the surface atoms. After CO_2 adsorption, both O1 and O2 oxygens of the CO_2 molecule lose charge density of $0.24e^-$ and $0.22e^-$, respectively, while surface copper atoms Cu_A and Cu_B which bind to these two oxygen atoms lose charge density of 0.12 and $0.10e^-$, respectively. However, the carbon atom gains $0.56e^-$ after binding to surface oxygen atom O_{SUF}, which loses $0.12e^-$. Hence, charge transfer has occurred to the CO_2 molecule from nearby surface atoms. As shown in Table XI, we note considerable changes in the frequencies of the different vibrational modes (υ_{as} = 1509, υ_s = 1281, and υ_b = 869 cm^{-1}) of the activated CO_2 molecule on this surface.

In another configuration (config. 2) the CO_2 molecule remains almost parallel to the surface, as shown in Fig. 13(b). The carbon atom binds to a top oxygen atom (O_{SUF}) (d_{C-OSUF} = 1.32 Å), while one oxygen (O1) of the CO_2 molecule binds to surface copper atoms Cu_A and Cu_B, with bond lengths 1.95 and 1.91 Å, respectively. The second oxygen atom (O2) of the molecule binds to another surface copper atom, Cu_C with a bond length of 1.91 Å. In the adsorbed CO_2 molecule we find O–C bond lengths of 1.32 and 1.27 Å for oxygen atoms O1 and O2, respectively, and the CO_2 angle is $\angle CO_2$ = 121.7°. The adsorption energy in this configuration is −98.7 kJ/mol, which is almost 40 kJ/mol less than in the

TABLE X. The adsorption energies and the characteristic parameter values of the CO_2 adsorbed geometry in the (2×2) supercell of $Cu_2O(001)$:Cu surface in config. 1 and config. 2.

Supercell	E_{ads} (kJ/mol)	$\angle CO_2$ (deg)	d_{C-O1} (Å)	d_{C-O2} (Å)	d_{O1-CuA} (Å)	d_{O1-CuB} (Å)	d_{O2-CuB} (Å)	d_{O2-CuC} (Å)	d_{C-OSUF} (Å)
Config. 1									
(2×2)	−138.1	121.5	1.29	1.28	1.85	...	1.87	...	1.35
Config. 2									
(2×2)	−98.7	121.7	1.32	1.27	1.95	1.91	...	1.91	1.32

TABLE XI. Vibrational frequencies (cm^{-1}) and Bader charges (e^-) comparison of the atoms in the adsorbed CO_2 molecule and Cu_2O(001):Cu surface atoms bonded with the molecule to that of in the isolated CO_2 molecule and the bare surface in config. 1 and config. 2 of (2×2) supercell.

Atoms and vibrational modes	C	O1	O2	Cu_A	Cu_B	Cu_C	O_{SUF}	υ_{as}	υ_s	υ_b
After CO_2 adsorption (config. 1)	1.52	−0.80	−0.82	0.46	0.44	...	−0.77	1509	1281	869
After CO_2 adsorption (config. 2)	1.86	−0.96	−1.11	0.59	0.61	0.65	−0.93	1461	1242	875
Isolated CO_2 molecule	2.08	−1.04	−1.04	...	...	...	...	2355	1316	632
Bare surface	...	...	...	0.34	0.34	0.51	−0.89	...	...	...

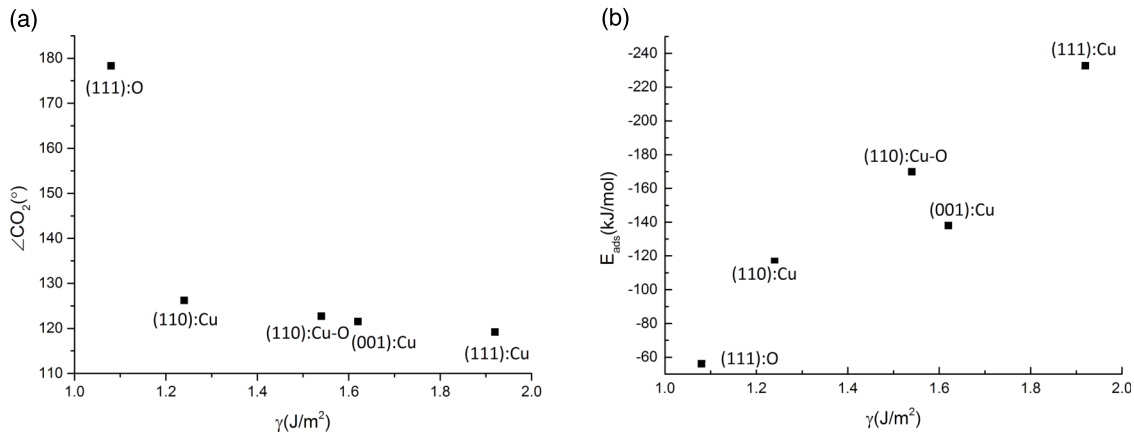

FIG. 14. The variation of CO_2 activation (∠OCO) (a) and adsorption energy (E_{ads}) (b) with surface energies of different surfaces. For the sake of simplicity we have plotted only lowest coverage values of only those configurations that show strongest binding with CO_2.

first configuration (Table X). The Bader charge analysis shows charge redistribution, with oxygen O1 losing $0.08e^-$ charge density, while the Cu_A and Cu_B atoms also lose $0.25e^-$ and $0.27e^-$, respectively. Oxygen atom O2 gains $0.07e^-$ charge density after binding to surface copper atom Cu_C, which loses $0.14e^-$. Charge transfer also occurs between surface oxygen atom, O_{SUF} and the C atom which gains $0.22e^-$, while O_{SUF} gains $0.04e^-$ (Table XI). Here again, we note considerable changes in the vibrational frequencies of the adsorbed CO_2 molecule, as shown in Table XI.

C. CO_2 adsorption trends in copper oxides

We noted that the activation of the CO_2 molecule is related to the adsorption energy, as shown in Fig. 14(a), where we considered the molecule's angle as a measure of its activation.[50] Furthermore, the adsorption energy, E_{ads}, depends almost linearly on the surface stability (Fig. 14(b)): The most stable (111):O surface shows weak adsorption (approximately −56 kJ/mol) and the CO_2 molecule remains linear, while the least stable (111):Cu surface shows the strongest binding (E_{ads} = −233 kJ/mol) with the CO_2 molecule bent to 119.2°. The second most stable surface, (110):Cu, shows an adsorption energy of approximately −117 kJ/mol, while the (001):Cu surface, binds the CO_2 molecule with the release of ∼138 kJ/mol, with the CO_2 molecule bending to 126.2 and 121.5°, respectively. This trend is similar to that found in CO_2 adsorption on CuO surfaces, where the most stable surface, (111), shows weak binding of the CO_2 molecule compared with other low index surfaces, which cause significant CO_2 activation.[11]

IV. SUMMARY AND CONCLUSIONS

Using DFT+U methodology, we have studied the reconstructions of the (111), (110), and (001) surfaces and proposed different non-polar terminations. We further analysed the structural geometries, energetics, and electronic properties for the process of carbon dioxide adsorption to different stoichiometric Cu_2O surfaces, at different coverages. While the CO_2 adsorption to stoichiometric Cu_2O(111):O is weak, causing no significant changes to the geometry or electronic structure of the adsorbate, CO_2 adsorption to all other surfaces is energetically favourable. The (110):Cu surface, which is only less stable by ∼0.16 J/m^2 compared to the most stable (111):O surface, shows adsorption energies up to approximately −117 kJ/mol, while the third most stable (110):Cu–O surface exhibits strong chemisorption of the CO_2 molecule, releasing ∼170 kJ/mol. We found that CO_2 coverage affects the adsorption energy as E_{ads} increases for all surfaces at lower coverage, where CO_2 is found to be chemisorbed as the CO_2^- anion. The Cu_2O(111) surface with Cu termination is found to be the least stable surface and a detailed structural and Bader charge analysis shows that the CO_2 molecule affects the surface geometry, rearranging itself to resemble a $[CO_3]^-$ species on the surface.

Activation of carbon dioxide is the most important step in its conversion into valuable chemicals and large structural transformations and significant charge transfer between different surfaces and the CO_2 molecule demonstrate that Cu_2O is capable of activating CO_2. For all the bent CO_2 configurations, we note a significant red-shift on the C–O symmetric (υ_s) and asymmetric (υ_{as}) stretching modes relative to the linear gas phase molecule, indicating that the

CO_2 molecule is considerably activated. It is worth noting, however, that our calculations are valid only at 0 K and only stoichiometric surfaces were considered in the present study. Nevertheless, the results presented in this paper provide fundamental mechanistic insights into CO_2 activation on stoichiometric (111), (110), and (001) surfaces, which will still be relevant to our general understanding of CO_2 adsorption by Cu_2O, as the different surfaces studied here include a wide variety of the kind of surface sites, that can be expected to occur on experimental surfaces.

SUPPLEMENTARY MATERIAL

The reconstructed unrelaxed surface structures of (111):Cu, (110):Cu, (110):CuO–O, and (001):Cu are given as Figs. S1–S4 in the supplementary material, respectively.

ACKNOWLEDGMENTS

This work was carried out as part of the Engineering and Physical Sciences Research Council (EPSRC) "4CU" programme grant, aimed at sustainable conversion of carbon dioxide into fuels, led by The University of Sheffield and carried out in collaboration with University College London, University of Manchester, and Queens University Belfast. The authors acknowledge the EPSRC for supporting this work financially (Grant Nos. EP/K001329/1 and EP/K035355/1). Via our membership of the UK's HEC Materials Chemistry Consortium, which is funded by EPSRC (Grant No. EP/L000202), this work used the ARCHER UK National Supercomputing Service (http://www.archer.ac.uk). The authors also acknowledge the use of the IRIDIS High Performance Computing Facility, and associated support services at the University of Southampton, in the completion of this work. N.H.d.L. thanks the Royal Society for an Industry Fellowship.

[1]Y. Hori, in *Modern Aspects of Electrochemistry*, edited by C. Vayenas, R. White, and M. Gamboa-Aldeco (Springer, New York, 2008), Vol. 42, Chap. 3, pp. 89–189.
[2]M. Gattrell, N. Gupta, and A. Co, J. Electroanal. Chem. **594**, 1 (2006).
[3]J. Szanyi and D. W. Goodman, Catal. Lett. **10**, 383 (1991).
[4]T. Matsumoto, R. A. Bennett, P. Stone, T. Yamada, K. Domen, and M. Bowker, Surf. Sci. **471**, 225 (2001).
[5]S. Y. Lee, N. Mettlach, N. Nguyen, Y. M. Sun, and J. M. White, Appl. Surf. Sci. **206**, 102 (2003).
[6]A. K. Mishra and N. H. de Leeuw, "Mechanistic insights into the Cu(I) oxide-catalyzed conversion of CO_2 to fuels and chemicals: A DFT approach," J. CO_2 Util. (in press).
[7]M. Le, M. Ren, Z. Zhang, P. T. Sprunger, R. L. Kurtz, and J. C. Flake, J. Electrochem. Soc. **158**, E45 (2011).
[8]G. Ghadimkhani, N. R. de Tacconi, W. Chanmanee, C. Janaky, and K. Rajeshwar, Chem. Commun. **49**, 1297 (2013).
[9]C. Wang, L. Yin, L. Zhang, D. Xiang, and R. Gao, Sensors (Basel) **10**, 2088 (2010).
[10]O. Lupan, V. Cretu, V. Postica, N. Ababii, O. Polonskyi, V. Kaidas, F. Schütt, Y. K. Mishra, E. Monaico, I. Tiginyanu, V. Sontea, T. Strunskus, F. Faupel, and R. Adelung, Sens. Actuators, B **224**, 434 (2016).
[11]V. Cretu, V. Postica, A. K. Mishra, M. Hoppe, I. Tiginyanu, Y. K. Mishra, L. Chow, N. H. de Leeuw, R. Adelung, and O. Lupan, J. Mater. Chem. **4**, 6527 (2016).
[12]A. K. Mishra, A. Roldan, and N. H. de Leeuw, J. Phys. Chem. C **120**, 2198 (2016).
[13]Z. K. Zheng, B. B. Huang, Z. Y. Wang, M. Guo, X. Y. Qin, X. Y. Zhang, P. Wang, and Y. Dai, J. Phys. Chem. C **113**, 14448 (2009).
[14]B. Z. Sun, W. K. Chen, and Y. J. Xu, J. Chem. Phys. **133**, 154502 (2010).
[15]C. Li, F. Wang, S. F. Li, Q. Sun, and Y. Jia, Phys. Lett. A **374**, 2994 (2010).
[16]B. Z. Sun, W. K. Chen, X. Wang, Y. Li, and C. H. Lu, Chin. J. Inorg. Chem. **24**, 340 (2008).
[17]W.-K. Chen, B.-Z. Sun, X. Wang, and C.-H. Lu, J. Theor. Comput. Chem. **7**, 263 (2008).
[18]H. Wu, N. Zhang, Z. Cao, H. Wang, and S. Hong, Int. J. Quantum Chem. **112**, 2532 (2012).
[19]H. Wu, N. Zhang, H. Wang, and S. Hong, Chem. Phys. Lett. **568-569**, 84 (2013).
[20]Y. Tan, X. Xue, Q. Peng, H. Zhao, T. Wang, and Y. Li, Nano Lett. **7**, 3723 (2007).
[21]M. Pang and H. C. Zeng, Langmuir **26**, 5963 (2010).
[22]Y. Sui, W. Fu, H. Yang, Y. Zeng, Y. Zhang, Q. Zhao, Y. Li, X. Zhou, Y. Leng, M. Li, and G. Zou, Cryst. Growth Des. **10**, 99 (2009).
[23]X. Zhao, Z. Bao, C. Sun, and D. Xue, J. Cryst. Growth **311**, 711 (2009).
[24]S. Sun, F. Zhou, L. Wang, X. Song, and Z. Yang, Cryst. Growth Des. **10**, 541 (2009).
[25]S. Sun, C. Kong, S. Yang, L. Wang, X. Song, B. Ding, and Z. Yang, CrystEngComm **13**, 2217 (2011).
[26]S. Sun, X. Song, Y. Sun, D. Deng, and Z. Yang, Catal. Sci. Technol. **2**, 925 (2012).
[27]E. L. Uzunova, N. Seriani, and H. Mikosch, Phys. Chem. Phys. **17**, 11088 (2015).
[28]L. I. Bendavid and E. A. Carter, J. Phys. Chem. C **117**, 26048 (2013).
[29]L. Wang, T. Maxisch, and G. Ceder, Phys. Rev. B **73**, 174112 (2006).
[30]L. Y. Isseroff and E. A. Carter, Phys. Rev. B **85**, 235142 (2012).
[31]M. Nolan and S. D. Elliott, Phys. Chem. Chem. Phys. **8**, 5350 (2006).
[32]D. O. Scanlon, B. J. Morgan, and G. W. Watson, J. Chem. Phys. **131**, 124703 (2009).
[33]C. E. Ekuma, V. I. Anisimov, J. Moreno, and M. Jarrell, Eur. Phys. J. B **87**, 23 (2014).
[34]G. Kresse and J. Hafner, Phys. Rev. B **47**, 558 (1993).
[35]G. Kresse and J. Hafner, Phys. Rev. B **49**, 14251 (1994).
[36]G. Kresse and J. Furthmüller, Comput. Mater. Sci. **6**, 15 (1996).
[37]G. Kresse and J. Furthmüller, Phys. Rev. B **54**, 11169 (1996).
[38]S. L. Dudarev, G. A. Botton, S. Y. Savrasov, C. J. Humphreys, and A. P. Sutton, Phys. Rev. B **57**, 1505 (1998).
[39]J. P. Perdew, K. Burke, and M. Ernzerhof, Phys. Rev. Lett. **77**, 3865 (1996).
[40]J. P. Perdew, K. Burke, and M. Ernzerhof, Phys. Rev. Lett. **78**, 1396 (1997).
[41]G. W. Watson, E. T. Kelsey, N. H. de Leeuw, J. D. Harris, and S. C. Parker, J. Chem. Soc., Faraday Trans. **92**, 433 (1996).
[42]P. W. Tasker, J. Phys. C: Solid State Phys. **12**, 4977 (1979).
[43]H. J. Monkhorst and J. D. Pack, Phys. Rev. B **13**, 5188 (1976).
[44]G. Wulff, Z. Kristallogr. **34**, 449 (1901).
[45]S. Grimme, J. Comput. Chem. **27**, 1787 (2006).
[46]A. Werner and H. D. Hochheimer, Phys. Rev. B **25**, 5929 (1982).
[47]A. Soon, M. Todorova, B. Delley, and C. Stampfl, Phys. Rev. B **75**, 125420 (2007).
[48]J. A. Assimos and D. Trivich, Phys. Status Solidi A **26**, 477 (1974).
[49]B. Z. Sun, W. K. Chen, X. Wang, and C. H. Lu, Appl. Surf. Sci. **253**, 7501 (2007).
[50]H. J. Freund and M. W. Roberts, Surf. Sci. Rep. **25**, 225 (1996).